J. Fluid Mech. (1983), *vol.* 135, *pp.* 283–299
Printed in Great Britain

Run-up of solitary waves

By G. PEDERSEN AND B. GJEVIK
Department of Mechanics, University of Oslo, P.O. Box 1053, Blindern, Oslo 3, Norway

(Received 23 March 1983)

A numerical model based on a Lagrangian description has been developed for studying run-up of long water waves governed by a set of Boussinesq equations. The performance of the numerical scheme has been tested by comparing with analytical solutions and experimental data. Simulations of the run-up of solitary waves on relatively steep planes (inclination angle $> 20°$) show surface displacements and run-up heights in good agreement with experiments. For waves with relatively large amplitude the simulations reveal the development of a breaking bore during the backwash. Results for run-up heights in converging and diverging channels are also presented.

1. Introduction

Large water waves generated either by seismic activity, landslides or avalanches have in many cases caused deaths and widespread destruction. The tsunami waves in the ocean and the destructive waves due to soil or snow slides in lakes or fjords are in many cases long waves, and the quasi-hydrostatic shallow-water theory may apply. In these large-scale wave phenomena, viscosity may be of minor importance, although the roughness of the sloping bottom may have a significant effect on the run-up. Wave amplification and run-up on sloping beaches have been the subject of numerous studies, and a general review can be found in Meyer & Taylor (1972). Various analytical solutions for run-up of long nonlinear waves on plane slopes have been given by Carrier & Greenspan (1958), Carrier (1966), Shuto (1967), Spielvogel (1976), Gjevik & Pedersen (1981) and Helal Badawi (1981). Experimental data on run-up of non-breaking waves are given among others by Hall & Watts (1953), Wiegel (1964), Kishi & Sacki (1967), Arntsen (1978) and Langsholt (1981). It is found that the run-up height is crucially dependent on the wave steepness and the slope of the plane. The calculations for the hydrostatic, non-viscous case done by Gjevik & Pedersen (1981) indicated that, for a solitary wave with amplitude A_s, $\kappa = (A_s/h_s)^{\frac{1}{2}} \cot\theta$ is the most important parameter for determining the run-up height R_s. In the expression for κ, θ denotes the inclination angle of the plane and h_s the undisturbed water depth away from the slope. The ratio R_s/A_s is a strictly increasing function of κ. The limit of R_s/A_s when κ tends to 0 is 2 and R_s/A_s is less than 2.1 for $\kappa < 0.3$. For $\kappa > 1$ the ratio becomes larger than 3. The run-up occurs in a wedge-shaped zone without any tendency for wave breaking when $A_s/h_s < 0.48(\tan\theta)^{\frac{10}{9}}$. For larger values of A_s/h_s the computations indicate that wave breaking may occur during the backwash. This breaking criterion was confirmed experimentally by Arntsen (1978) and Langsholt (1981).

The analytical solutions proposed so far for modelling long-wave run-up are based on several simplifications, and the effects of these approximations are difficult to estimate. For this reason we have applied numerical methods to solve the inviscid

nonlinear shallow-water equation including also non-hydrostatic effects. We have developed a model for waves propagating along the longitudinal axis of a channel of varying cross-sectional area and with a sloping beach at the end (§2). Owing to the moving free surface the numerical treatment of the shoreline boundary becomes difficult in a finite-difference representation based on an Eulerian description. This problem may be overcome in various ways – see for example Hibberd & Peregrine (1979) in their study of run-up of bores.

In this paper we shall use a Lagrangian coordinate description which simplifies the numerical treatment of the moving shoreline. In order to model nonlinearity, dispersion and the boundary conditions properly, we have developed an implicit numerical scheme for this problem (§3). The performance of this scheme has been investigated by linear stability analysis and by comparing with the nonlinear analytical solutions given by Spielvogel (1976).

Viscosity will of course always be important at the tip of the water wedge and will therefore have some effect on the run-up height. As long as the bulk of the water wedge is relatively thick compared with the boundary layer, inviscid theory may apply, and we therefore expect that viscosity is of minor importance for relatively steep slopes. The good agreement that is found between the numerical simulations and the experiments for inclination angles $\theta > 20°$ supports this suggestion (§4).

2. Basic equations

We shall derive the equation of motion in Lagrangian description for long gravity waves in a channel with a sloping beach at the end. Cartesian axes $Oxyz$ are introduced with the origin in the undisturbed free surface, Ox directed along the channel, Oy across the channel and Oz vertical, as indicated in figure 1. The cross-sectional area $S(x,t)$ of the channel filled with water is a function of x and time t, and the total water depth is $H(x,y,t)$. It is convenient to write $H = h+\eta$, where $h = h(x,y,t)$ is the depth reckoned from the undisturbed water level and $\eta = \eta(x,y,t)$ is the displacement of the water surface. With h as a function of time we also allow for the possibility that the bottom topography may change in time.

The density ρ of the water, the acceleration g due to gravity, a typical undisturbed depth h_s of the water, and a typical wavelength λ_s are used to introduce a velocity scale $c_s = (gh_s)^{\frac{1}{2}}$, a timescale $t_s = \lambda_s/c_s$ and a pressure scale $p_s = \rho c_s^2$. We assume that $h_s \ll \lambda_s$ and introduce a small parameter $\epsilon = (h_s/\lambda_s)^2$. The width and the depth of the channel are considered to be of the same order, and the variation of the width is of order $\epsilon^{\frac{1}{2}}$. Hence we define dimensionless variables as follows:

$$(x,y,z) = \left(\frac{x^*}{\lambda_s}, \frac{y^*}{h_s}, \frac{z^*}{h_s}\right), \quad (u,v,w) = \left(\frac{u^*}{c_s}, \frac{v^*}{\epsilon^{\frac{1}{2}}c_s}, \frac{w^*}{\epsilon^{\frac{1}{2}}c_s}\right),$$

$$t = \frac{t^*}{t_s}, \quad H = \frac{H^*}{h_s}, \quad p = \frac{p^*}{p_s}, \quad \eta = \frac{\eta^*}{h_s},$$

where $*$ indicates a dimensional variable, u, v, and w denote the velocity components in the x-, y- and z-directions, and p is the pressure. With this scaling, the equation of motion, the continuity equation and the condition of irrotational flow can be expressed in the form given in Appendix A. By retaining only the terms of order ϵ, we obtain the shallow-water approximation

$$\mathrm{D}\bar{u} = -\tilde{\eta}_x + \epsilon Q, \tag{2.1}$$

$$\mathrm{D}S = -S\bar{u}_x, \tag{2.2}$$

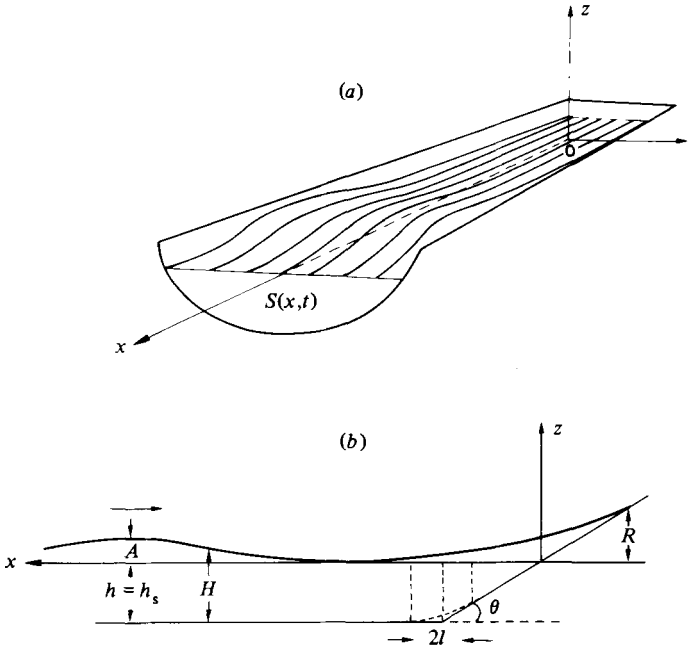

FIGURE 1. Sketch of channel with symbol definition: (*a*) plane cut through the longitudinal axis of the channel (*b*).

where $\mathrm{D} = \partial/\partial t + \bar{u}\,\partial/\partial x$, and subscript x denotes differentiation with respect to x. The mean velocity $\bar{u}$ and the mean surface displacement $\tilde{\eta}$, which are functions of x and t only, are defined in Appendix A. The mean values denoted by $\sim$ and $-$ are free-surface average and cross-sectional average respectively. Q represents a first-order correction to the hydrostatic pressure gradient $\tilde{\eta}_x$. In Appendix A we describe a method by which Q can be evaluated for different shapes of the cross-section of the channel. For a symmetric rectangular cross-section the mean value $\tilde{\eta} = \bar{\eta} + O(\epsilon^2)$, and we find

$$Q = -\tfrac{1}{3}b_x \mathrm{D}^2 b + \tfrac{1}{6}[\bar{H}(\mathrm{D}^2\bar{H})_x - \bar{H}_x \mathrm{D}^2\bar{H}] - \tfrac{1}{2}[(\bar{H}\,\mathrm{D}^2\bar{\eta})_x - \bar{\eta}_x \mathrm{D}^2\bar{H}] - \bar{\eta}_x \mathrm{D}^2\bar{\eta}, \qquad (2.3)$$

where $2b$ is the width of the channel. In (2.3) we have retained the nonlinear terms since some of these terms might have an effect on the run-up of strongly nonlinear waves. Another reason for keeping the nonlinear form of Q is that this leads to a simpler analytical expression for the solitary wave. The linearized version of Q is normally used in the Boussinesq equation.

It is also possible to evaluate Q for channels with triangular cross-section. Details are given in Appendix A.

For a channel with rectangular cross-section we shall introduce a mean Langrangian coordinate defined by $x = x(a, t)$, where a is the initial coordinate of the fluid particle. Hence

$$x_t = \bar{u}, \qquad (2.4)$$

where subscript t denotes differentiation with respect to time. In Lagrangian description of continuity equation (2.2) can be integrated with respect to time, and

this leads to $Sx_a = S_0$, where S_0 is the initial cross-sectional area with the corresponding averaged water depth H_0. Equation (2.2) can therefore be written in the form

$$\overline{H}_t = q = -\overline{H}\left(\frac{b_x}{b}\bar{u} + \frac{S}{S_0}\bar{u}_a\right). \tag{2.5}$$

In order to find the final expression for the equation of motion in Lagrangian coordinates we substitute $\bar{\eta} = \overline{H} - h$ in (2.3). This leads to a simpler implementation of the shoreline boundary condition. In general three types of nonlinear terms will appear: terms that are products of velocities ($\bar{u}$, q etc.), terms that are products of the displacement ($\overline{H}$, $\overline{H}_x$ etc.), and finally products of velocity and displacement. We may expect that the latter terms will be the most important during the run-up, and we have therefore neglected terms of the first type. Numerical experiments with different forms of Q have justified this assumption and shown that the effect on the run-up heights is negligible for the cases reported below (Pedersen 1981). This gives the following expression for Q:

$$Q = (\tfrac{1}{2}\overline{H}h_{xx} - \tfrac{1}{2}\overline{H}h_x b_x/b - \tfrac{1}{3}b_x^2)\,\mathrm{D}\bar{u} - \tfrac{1}{3}\overline{H}(\mathrm{D}^2\overline{H})_x - \tfrac{2}{3}\overline{H}_x\,\mathrm{D}^2\overline{H}.$$

This expression is identical with (2.3) if h and b are constant, and therefore gives the same solitary-wave solution.

The fully linearized version of Q is obtained by substituting h for $\overline{H}$, h_x for $\overline{H}_x$, $\bar{\eta}_{tt} + h_x\bar{u}_t$ for $\mathrm{D}\overline{H}$ and $\bar{u}_t$ for $\mathrm{D}\bar{u}$ in the last equation. (All partial derivation is done with respect to Eulerian coordinates.) Linearizing of $\mathrm{D}\bar{u}$ and $\mathrm{D}\overline{H}$ is of no use since such terms are automatically linearized by the transformation to Lagrangian coordinates. On the contrary, by using the approximation to Q given above, the Lagrangian description will be fully consistent with the Eulerian without inclusion of awkward and 'un-Langrangian' terms of the form $\bar{u}\bar{u}_a$. Hence the equation of motion in Langrangian description reads

$$\left[1 + \epsilon\left(\tfrac{1}{3}b_x^2 + \tfrac{1}{2}h_x\frac{b_x}{b} - \tfrac{1}{2}\overline{H}h_{xx}\right)\right]\bar{u}_t = -\frac{S}{S_0}\overline{H}_a + h_x - \frac{\epsilon}{3}\frac{S}{S_0}(\overline{H}q_{at} + 2\overline{H}_a q_t). \tag{2.6}$$

For reasons that will be explained in §3, $\overline{H}_t = q$ has been kept as an independent variable in (2.5) and (2.6). More details concerning the transformation to Lagrangian coordinates are given in Appendix B.

For a rectangular channel of constant width and depth $h = 1$ the Boussinesq equations (2.1) and (2.2) with K defined by (2.3) possess a solitary-wave solution

$$\bar{\eta} = A\,\mathrm{sech}^2\,p(x + ct - x_0), \tag{2.7}$$

$$\bar{u} = \frac{-c\bar{\eta}}{1+\bar{\eta}}, \tag{2.8}$$

where A is the dimensionless amplitude (scaled by h_s), $c = (1+A)^{\frac{1}{2}}$, $p = (3A/\epsilon)^{\frac{1}{2}}/2c$, and x_0 is the initial position of the wave crest. In Lagrangian coordinates there is of course a corresponding solitary-wave solution to (2.4)–(2.6). This expression is most easily obtained by transforming the solution (2.7) and (2.8) to Langrangian coordinates (a, t). Details are given by Pedersen (1981). Far away from x_0 the solitary wave is described by the following implicit relation

$$\frac{\sqrt{3}}{c}|a + ct - x_0| = 2f - \frac{1}{A^{\frac{1}{2}}}\ln\frac{A^{\frac{1}{2}} - f}{A^{\frac{1}{2}} + f}, \tag{2.9}$$

where $f = (A - \bar{\eta})^{\frac{1}{2}}$. For given values of a and t, $\bar{\eta}$ can be obtained by solving (2.9) numerically, and the corresponding mean particle velocity $\bar{u}$ can be found from (2.8).

In the numerical simulations, we generated a shoreward-moving solitary wave by specifying the mean horizontal velocity $\bar{u}_w(t)$ of a horizontally moving wall far away from the shoreline. The boundary condition at the wall will be

$$\bar{u} = \bar{u}_w(t) \quad (a = a_w), \tag{2.10}$$

where a_w is the initial position of the wall and $\bar{u}_w(t)$ is determined from (2.9) and (2.8).

At the shoreline we always have

$$\bar{H} = q = 0 \quad (a = a_s), \tag{2.11}$$

where a_s is the initial position of the shoreline. For a rectangular channel the ratio S/S_0 is finite provided that $\bar{H}/H_0$ is finite. We note that, as long as wave breaking does not occur, the ratio $\bar{H}/H_0$ is finite even at the shoreline where $\bar{H}$ and H_0 are both zero. This is easily seen by applying L'Hôpital's rule, which leads to the requirement η_x finite and $H_{0a} \neq 0$ for $a = a_s$.

3. Numerical methods

For convenience we shall drop the overbar for the mean values $\bar{H}$ and $\bar{u}$. The equations (2.4)–(2.6) are solved numerically on a space-staggered grid by a second-order finite-difference scheme which is implicit in space. We denote a space and time increments by Δa and Δt respectively, the numerical approximation to a variable F at $a = j\Delta a$, $t = n\Delta t$ by F_j^n, and we define the differences $\partial_t F_j^n = F_j^{n+1} - F_j^n$ and $\partial_a F_j^n = F_{j+1}^n - F_j^n$. Hence the finite-difference equation corresponding to (2.5) can be written

$$\partial_t H_j^n = \tfrac{1}{2}\Delta t(\hat{q}_j + q_j^n) = -\frac{\Delta t}{2} H_j^+ \left[\frac{1}{2}\left(\frac{b_x^+}{b^+}\right)_j (u_{j-\frac{1}{2}}^{n+1} + u_{j+\frac{1}{2}}^{n+1} + u_{j-\frac{1}{2}}^n + u_{j+\frac{1}{2}}^n) + \frac{S_j^+}{\Delta a S_{0j}} (\partial_a u_{j-\frac{1}{2}}^n + \partial_a u_{j-\frac{1}{2}}^{n+1})\right], \tag{3.1}$$

where $H_j^+ = H_j^n + \frac{1}{2}\Delta t q_j^n$. A similar extrapolation is used for the other variables. The predictor value for q_j^{n+1}, $\hat{q}_j$ is introduced in order to avoid instabilities in regions with large stretching of the fluid elements which may occur at the top of the water tongue near the shoreline. Similarly the finite-difference equation corresponding to (2.6) reads

$$E\,\partial_t u_{j+\frac{1}{2}}^n = \tfrac{1}{2}B(\partial_a H_j^n + \partial_a H_j^{n+1}) + \Delta t(h_x)_{j+\frac{1}{2}}^+ - C(\partial_a \hat{q}_j - \partial_a q_j^n) - \tfrac{1}{2}D(\hat{q}_{j+1} + \hat{q}_j - q_{j+1}^n - q_j^n), \tag{3.2}$$

where E, B, C and D are the coefficients in (2.6) extrapolated as H_j^+ and multiplied by appropriate powers of Δa and Δt. The numerical representation of h_x, $(h_x)_{j+\frac{1}{2}}^+$, is defined by

$$(h_x)_{j+\frac{1}{2}}^+ = \frac{1}{2\Delta x}[h(x_{j+\frac{1}{2}}^+ + \Delta x) - h(x_{j+\frac{1}{2}}^+ - \Delta x)],$$

where Δx is chosen suitably in order to match the numerical representation of the term h_x to the first term on the right-hand side of (3.2). In the numerical simulation reported in this paper $\Delta x = \frac{1}{4}(x_{j+1}^+ - x_{j-1}^+)$ with an appropriate modification at the shoreline. From (3.1) and (3.2) we eliminate H^{n+1} and $\hat{q}$ and solve a tridiagonal set for u^{n+1}. Hence H^{n+1} can be determined from (3.1).

The x-values at $t = (n+1)\Delta t$ are obtained from the kinematic relation (2.4), which in finite-difference form reads

$$\partial_t x_{j+\frac{1}{2}}^n = \tfrac{1}{2}\Delta t(u_{j+\frac{1}{2}}^{n+1} + u_{j+\frac{1}{2}}^n).$$

The final values of q are then calculated by

$$q_j^{n+1} = -H_j^{n+1}\left[\frac{1}{2}\left(\frac{b_x}{b}\right)_j (u_{j+\frac{1}{2}}^{n+1} + u_{j-\frac{1}{2}}^{n+1}) + \frac{S_j^{n+1}}{\Delta a\, S_{0j}} \partial_a u_{j-\frac{1}{2}}^{n+1}\right].$$

Lateral boundary conditions at the shoreline and at the horizontally moving wall are now easily implemented. The grid is arranged such that the wall is located at the grid point where x and u are specified, and the shoreline is located at a grid point for H and q. The wall boundary condition (2.10) becomes

$$u_{m+\frac{1}{2}}^n = u_w(n\Delta t) \quad (a = a_w),$$

where $a_w = (m+\frac{1}{2})\Delta a$ is the initial position of the wall. The shoreline boundary conditions (2.11) read

$$H_p^n = \hat{q}_p = q_p^n = 0.$$

For the linearized equations (2.4)–(2.6) with constant width and constant depth $h = 1$ the stability and dispersion properties of the numerical scheme can be investigated by standard methods (Meisinger & Arakawa 1976). For a sinusoidal wave with wavenumber k and angular frequency ω we find the dispersion relation

$$\sin^2(\tfrac{1}{2}\omega\Delta t) = \left(\frac{\Delta t}{\Delta a}\right)^2 \frac{\sin^2(\frac{1}{2}k\Delta a)}{1 + (\frac{1}{3}+\frac{1}{4}(\Delta t)^2)\sin^2(\frac{1}{2}k\Delta a)/(\frac{1}{2}\Delta a)^2}. \tag{3.3}$$

It is easily seen that ω is real for all values of k, Δa and Δt, which implies that the scheme is unconditionally stable. For long waves we get

$$\omega = k[1 - \tfrac{1}{6}k^2(1 + \tfrac{1}{2}(\Delta t)^2 + \tfrac{1}{4}(\Delta a)^2)] + O(k^4).$$

With Δt and $\Delta a \ll 1$, the scheme models the dispersion properties for long waves well. Figure 2 shows a comparison between phase velocity obtained from (3.3) and the phase velocity $c = \omega/k = (1+\frac{1}{3}k^2)^{-\frac{1}{2}}$ obtained by the analytical solution of the linearized Boussinesq equations.

The performance of the scheme in the nonlinear case is checked in two ways. Solitary waves are found to propagate with constant speed, amplitude and shape in close agreement with analytical results. By retaining only hydrostatic effects in (3.2), i.e. $C = D = 0$, $E = 1$ and $B = -H/H_0$, we may also compare with Spielvogels' (1976) analytical results for run-up of nonlinear waves on a sloping plane. The results of the comparison are displayed in figure 3.

For small-amplitude waves propagating along a channel of uniform depth and exponentially varying width, it is possible to obtain a simple analytical solution to (2.4)–(2.6) which may be compared with numerical results. We set $h = 1$ and $b = b_0 e^{-\alpha x}$, where α is a constant. The linearized form of (2.5) and (2.6) is

$$\eta_t = \alpha u - u_a, \quad u_t = -\eta_a,$$

where we have neglected the non-hydrostatic terms and the overbar. These equations have solutions

$$(u, \eta) = (u_0, \eta_0)\, e^{pa}\, e^{i(ka+\omega t)},$$

where u_0, η_0, p, k and ω are constants, $p = \frac{1}{2}\alpha$ and $\omega = \omega_a = k(1+\alpha^2/4k^2)^{\frac{1}{2}}$. The numerical scheme leads to a corresponding numerical solution with

$$p = \tfrac{1}{2}\alpha + \tfrac{1}{24}\alpha^3(\Delta a)^2 \ldots,$$

$$\omega = \omega_a\left[1 - \left(\frac{\Delta a k}{\omega_a}\right)^2\left(\frac{\alpha^2}{16} + \frac{\alpha^4}{128k^2} + \frac{k^2}{24}\right) - \frac{\Delta t^2}{12}\omega_a^2 \ldots\right].$$

A stable solution with real ω is possible only when $\frac{1}{2}(\Delta a)\,\alpha = \frac{1}{2}(\Delta a)\, b_x/b < 1$.

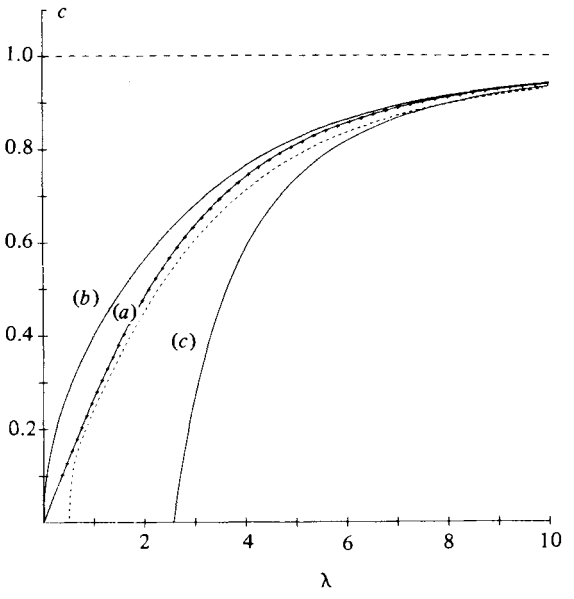

FIGURE 2. Phase velocity c as function of wavelength $\lambda = 2\pi/k$. Full drawn lines: (a) dispersion relation for the linearized Boussinesq equations, $c = (1+\frac{1}{3}k^2)^{-\frac{1}{2}}$; ($b$) exact dispersion relation for linear gravity waves $c = (\tanh k/k)^{\frac{1}{2}}$; ($c$) dispersion relation for the linearized KdV equation, $c = 1-\frac{1}{6}k^2$. Results from the stability analysis of the numerical scheme (3.3): + + + +, $\Delta a = \Delta t = 0.1$; — — — —, $\Delta a = \Delta a = 0.5$.

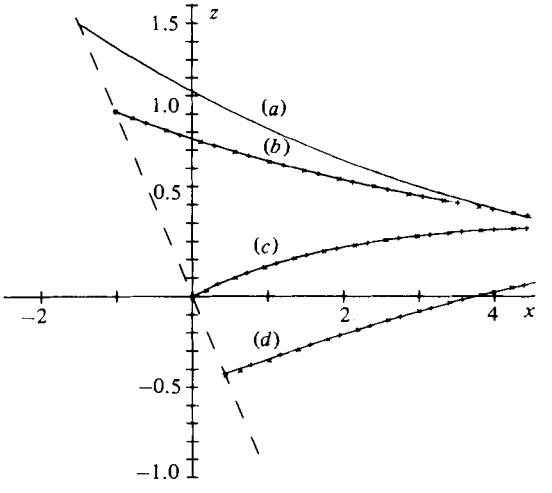

FIGURE 3. Comparison with Spielvogel's analytical results (full drawn lines). (a) Initial position of water surface. (b), (c), (d) Subsequent positions of water surface at intervals of 1.94 time units. Results of numerical simulations: + + + +, $\Delta a = \Delta t = 0.1$; × × × ×, $\Delta a = \Delta t = 0.5$.

In general the scheme will not preserve energy and volume exactly. Typical values for change of volume in the simulations reported in this paper are 0.01–0.1‰ of the total volume transport through a cross-section far away from the shoreline. The energy changes are 0.01–0.1‰ of the total energy input by the generation of the solitary wave.

4. Results of the simulations. Comparison with experiments

Simulations of run-up of solitary waves on an inclined plane have been performed with the geometry shown in figure 1 (*b*). The first sets of simulations are two-dimensional corresponding to the wave motion in a channel with rectangular cross-section and constant width. As explained previously in §2, the solitary wave is generated by prescribing the mean horizontal velocity at a position sufficiently far away from the shoreline for the primary run-up and backwash not to be disturbed by reflections from the wave generator. In view of the appearance of higher-order derivatives of $h(x)$ in (2.6), the transition between the flat bottom and the inclined plane was smoothed. The smoothing extended over an interval of length $2l$ centred at $x = \cot\theta$, where θ is the inclination angle of the plane. Hence we defined the water depth by

$$h(x) = 1 - l\tan\theta\, p(s),$$

where p is the polynominal of lowest possible degree that satisfies the boundary conditions $p(1) = p'(1) = 1$, $p''(1) = p'''(1) = 0$ and $p(-1) = p'(-1) = p''(-1) = p'''(-1) = 0$, namely

$$p(s) = \tfrac{1}{32}(s^6 + 5s^4 + 15s^2 - 16s + 5)$$

and $s = (x + \cot\theta)/l$. Numerical experiments with different values of l showed that with $l < 0.25\cot\theta$ the smoothing had only minor effects (usually less than 0.5%) on the run-up heights (Pedersen 1981). For very small values of l compared with the grid size, local disturbances in the flow field appeared near $x = \cot\theta$. In the simulations reported below we have used $l = 0.25\cot\theta$.

Figure 4 (*a*) shows simulated run-up of a solitary wave with amplitude $A = 0.3$ on a plane inclined an angle 20° to the horizontal direction. The computed surface displacement may be compared with the time-lapse photographs (figure 4*b*) of a corresponding run-up experiment by Langsholt (1981).

Langsholt's experiment was carried out in a 15 m long and 0.5 m wide wave tank. A nonlinear single-crested wave was generated by a wavemaker at the end of the tank, and measuring probes along the tank showed that the wave developed into a form corresponding closely to a solitary wave except for some distortions at the tail. By comparing figures 4 (*a*) and 4 (*b*) we see that there is a close agreement between the numerical and the experimental results. The experiments show that a steep front developed during the backwash (figures 4*b*, *f*), which eventually leads to breaking (figures 4*b*, *g*). The steepening is reproduced very well by the numerical simulation (figures 4*a*, *f*), but the breaking process is of course beyond the scope of the present theory. The formation of backwash bores has also been observed in numerical simulation of wave run-up by Hibberd & Peregrine (1979).

Figure 5 (*a*) shows the simulated run-up of a solitary wave with amplitude $A = 0.19$ on a plane inclined at an angle $\theta = 30°$ to the horizontal direction. In order to compare these results with experimental data we have performed an experiment with the same experimental set-up as used by Langsholt but with an improved wave generator. This led to a wave corresponding more closely to the solitary-wave form, but there were some distortions at the tail. Time-lapse photographs of the run-up are shown in figure

5(*b*). As in the previous case, a correct comparison between experiments and numerical simulations requires that the position of the peak amplitude of the incoming wave (figures 5*b*, *a*) can be determined very accurately. With the equipment we used this is difficult and it may introduce an error. A control of the camera also showed that the time interval between each photograph varied slightly within the range 0.45 ± 0.02 s. A detailed comparison between figures 5(*a*) and (*b*) shows, however, that within the error limits the agreement is excellent. In this case breaking was not observed.

We expect that breaking during backwash occurs for small values of θ and large values of A. Based on simplified analytical solutions, Gjevik & Pedersen (1981) obtained a breaking criterion for solitary waves

$$A \geqslant 0.48(\tan\theta)^{\frac{10}{9}},$$

which was found to correspond well with observations. This criterion indicates that for $\theta = 20°$ and $\theta = 30°$ breaking will occur for $A \geqslant 0.16$ and $A \geqslant 0.26$ respectively, which is in good agreement with the experimental and numerical results in figures 4 and 5.

The maximum run-up height R obtained from numerical simulations may also be compared with measurements. Hall & Watts (1953) (see Wiegel 1964) found by a best fit to experimental data that R (scaled by h_s) depends on the wave amplitude A according to the formula

$$R = KA^{\alpha}, \tag{4.1}$$

where K and α are functions of the inclination angle θ. For $\theta = 20°$ this relation is depicted in figure 6 with the values of K and α given by Hall & Watts. These results are confirmed by the measurements of Langsholt (1981). The numerical simulations indeed show that a relation of the form (4.1) exists, but the value $K = 3.88$ obtained numerically is somewhat higher than the value $K = 3.48$ found experimentally by Hall & Watts.

Figure 7 shows numerical and experimental values of K and α for different values of θ. The numerical results compare well with the experimental data for $\theta > 20°$. The discrepancy between the numerical simulations and experiments for smaller values of θ is most likely due to surface tension and frictional effects which are neglected in the present theory. Langsholt's data for different water depths show that K depends on water depth and that the data for $h_s = 25$ cm are in much better agreement with the numerical results than are his data for $h_s = 15$ cm and $h_s = 10$ cm. The significant increase in the value of K for water depths between 15 and 25 cm for $\theta < 20°$ confirms that frictional effects become less important in deep channels.

Based on the analytical expression for run-up heights given by Gjevik & Pedersen (1981), it is possible to estimate the thickness of the viscous boundary layer along the plane and compare it with the thickness of the water wedge.

The region close to the tip where the boundary layer is of comparable thickness to the water depth is small if the Reynolds number $Re = c_s h_s/\nu$ is much larger than a certain value Re_c. The value of Re_c depends in a rather complicated way on wave amplitude A and inclination angle θ. A rough estimate for Re_c can be found from standard theory for turbulent boundary layers. The boundary-layer thickness is calculated from the average run-up velocity along the plane deduced from the results given by Gjevik & Pedersen (1981). The velocities were assumed to vary slowly enough for the steady-state approximation to be used and the effect of the free surface was neglected. Re^* is defined as the value of Re for which the boundary-layer thickness calculated in the above manner is equal to or larger than the total water depth over

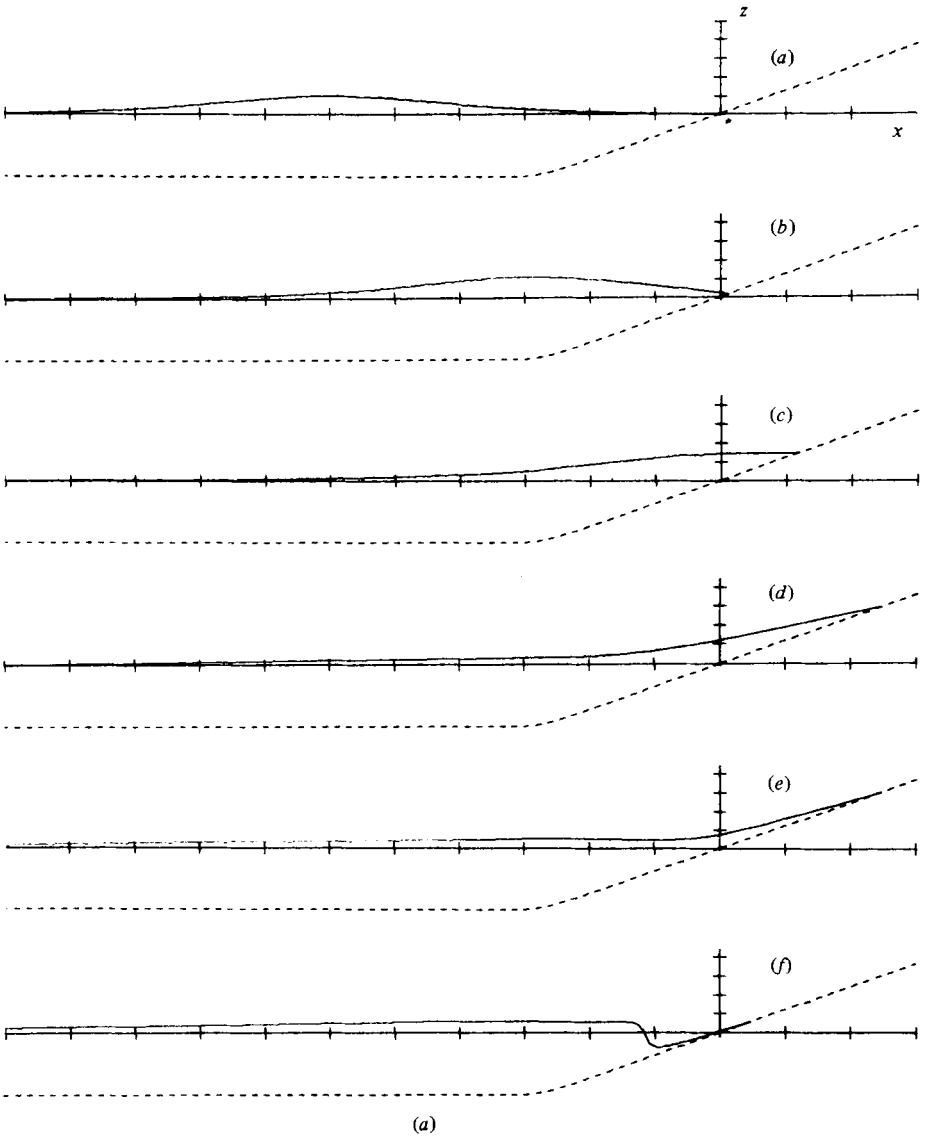

(a)

FIGURE 4(a). For caption see facing page.

5 % of the run-up length. Even though the free-surface effect cannot be neglected close to the tip, we believe that Re^* at least will give some indication of the magnitude of Re_c. Generally Re^* will increase sharply for decreasing values of θ. We find for example with $A = 0.2$, $Re^* \approx 10^4$ for $\theta = 20°$ and $Re^* \simeq 10^5$ for $\theta = 15°$. These rough estimates indicate that for water depth h_s of about 25 cm ($Re = 3 \times 10^5$) frictional effects may be of minor importance for $\theta > 15°$.

For the same reasons we may expect that in large-scale experiments or geophysical phenomena the run-up heights are in better agreement with the numerical predictions even for values of $\theta < 15°$.

Propagation of long waves in diverging and converging channels has been studied in papers by Miles (1979) and Chang, Melville & Miles (1979). We will briefly report

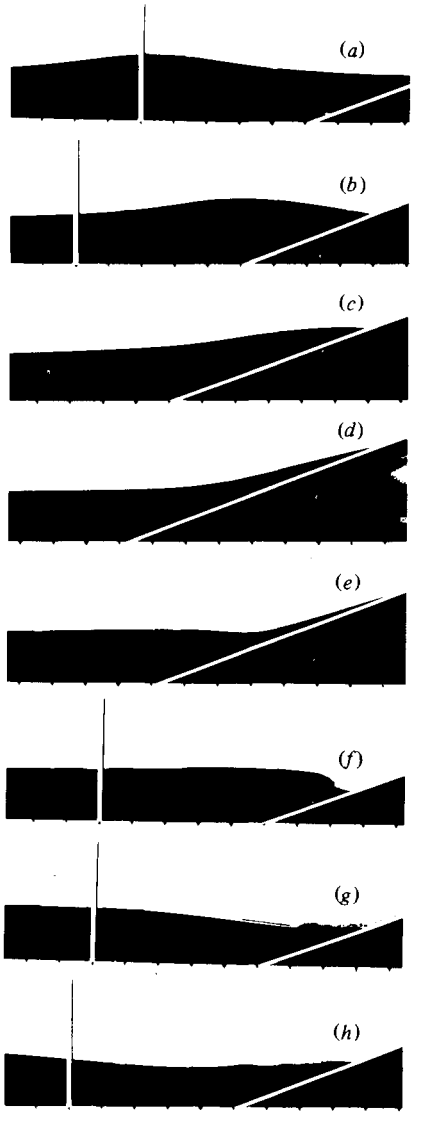

(*b*)

FIGURE 4. (*a*) Numerical simulations of run-up of a solitary wave with amplitude $A = 0.3$ on an inclined plane $\theta = 20°$. (*a*)–(*f*) surface displacement at time intervals 2.7 time units. (*b*) Time-lapse photographs of run-up of a solitary wave in a wave tank. $A = 0.3$, $\theta = 20°$, water depth $h_s = 0.15$ m. (*a*)–(*h*) at time intervals 0.33 s or 2.7 time units.

some simulations of run-up in channels with varying width. Such simulations may be of interest for studies of the propagation of large waves generated by slides or avalanches in fjords and lakes. In the simulations the half-width $b(x)$ of the channel was varying in the same way as the depth $h(x)$; $b = \frac{1}{2}$ for $x + \cot\theta < -l$, and $b = \frac{1}{2} - (x + \cot\theta)\tan\psi$ for $x + \cot\theta > l$, and smoothed in an analogous way to h in the intermediate interval. ψ is the angle between the vertical lateral walls and the x-direction. Some results for $\theta = 15°$ are displayed in figure 8, which shows that the relative change of the run-up R with ψ is significant and that there is an asymmetry

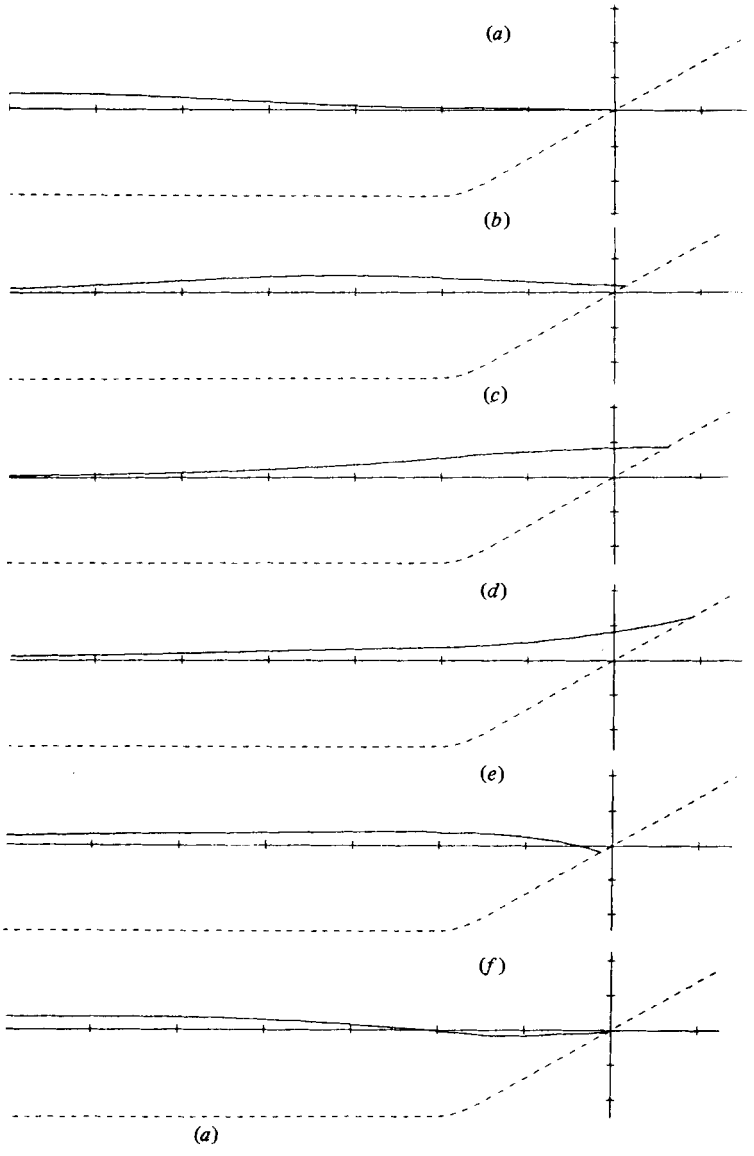

FIGURE 5(a). For caption see facing page.

with respect to positive and negative values of ψ i.e. for converging and diverging channels. A similar effect was found by Chang *et al.* (1979) for solitary-wave propagation in diverging and converging channels of uniform depth.

The authors wish to thank Mr Arve Kvalheim and Mr Olav Hånde for helpful assistance with the laboratory experiments.

Appendix A

The shallow-water equations including non-hydrostatic effects have been derived for uniform channels by Peters (1966) and Peregrine (1968). We shall extend this theory to the case with varying cross-section. With the notation and scaling

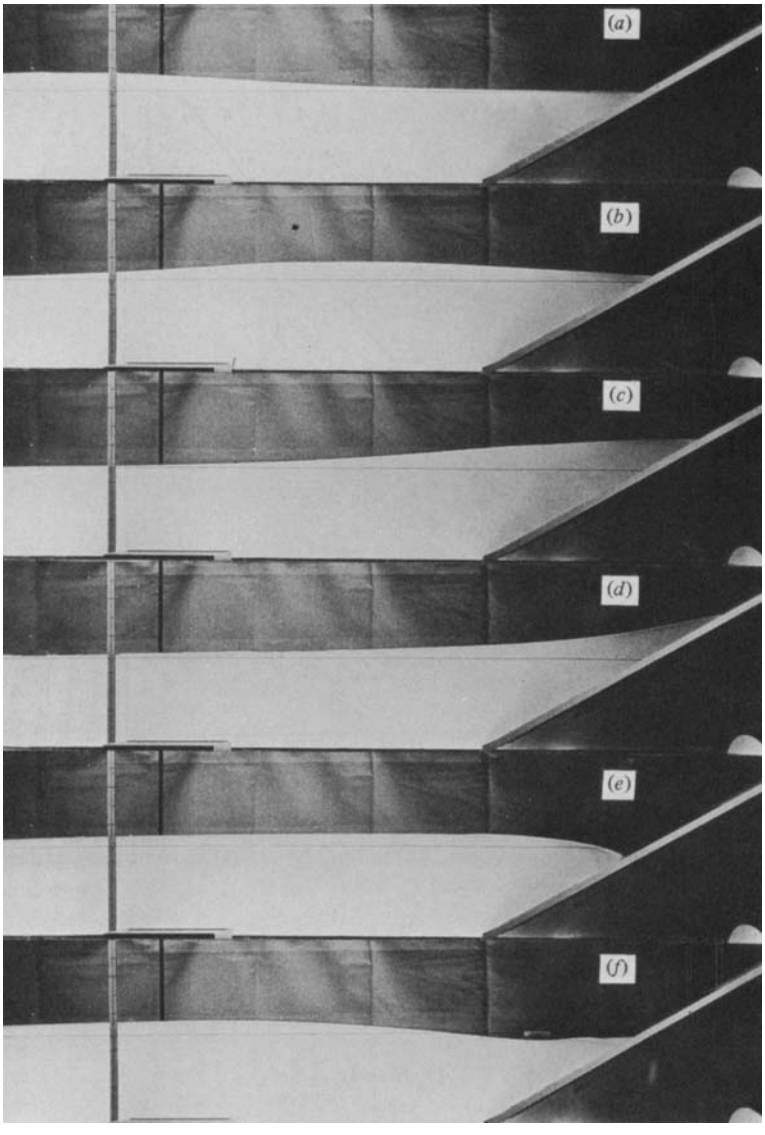

FIGURE 5. (*a*) Numerical simulations of run-up of a solitary wave with amplitude $A = 0.19$ on an inclined plane $\theta = 30°$. (*a*)–(*f*) surface displacement at intervals 2.86 time units. (*b*) Time-lapse photographs of run-up of a solitary wave in a wave tank. $A = 0.19$, $\theta = 30°$, water depth $h_s = 0.24$ m. (*a*)–(*f*) at time intervals 0.45 s $\pm$ 0.025 s or $\sim$ 2.86 time units.

introduced in §2, the equation of motion and the continuity equation for an inviscid incompressible fluid read

$$\mathrm{D}_3 u = -p_x, \quad \epsilon\,\mathrm{D}_3 v = -p_y, \quad \epsilon\,\mathrm{D}_3 w = -p_z - 1, \tag{A 1}$$

and

$$u_x + v_y + w_z = 0, \tag{A 2}$$

where the operator $\mathrm{D}_3 = \partial/\partial t + u\,\partial/\partial x + v\,\partial/\partial y + w\,\partial/\partial z$, and an independent variable as subscript denotes differentiation with respect to this variable. Irrotational motion implies that

$$u_y - \epsilon v_x = u_z - \epsilon w_x = v_z - w_y = 0. \tag{A 3}$$

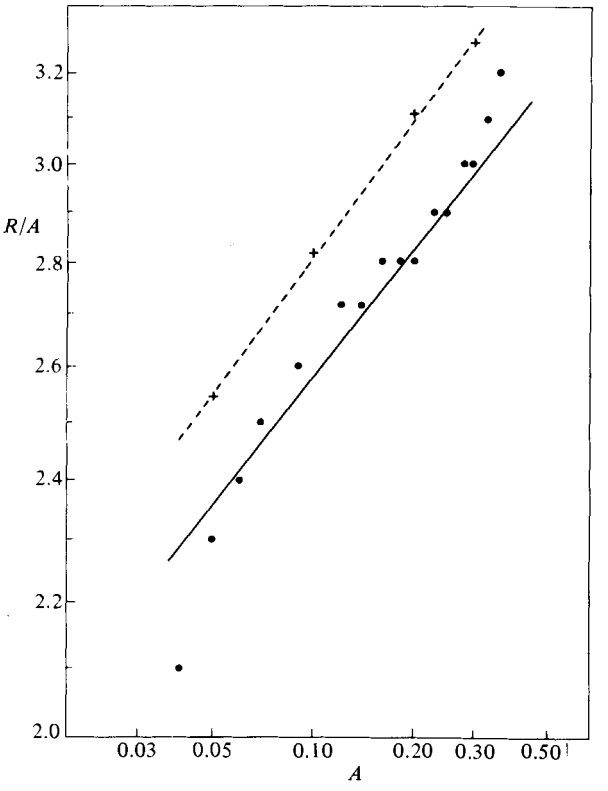

FIGURE 6. Run-up for a solitary wave with amplitude A on a plane inclined an angle $\theta = 20°$. Full drawn line shows experimental results by Hall & Watts ($K = 3.48$, $\alpha = 1.13$); ●, Langsholt's results; +, results of numerical simulations. Dotted line shows best fit to numerical data. ($K = 3.88$, $\alpha = 1.14$).

The boundary of the fluid is defined by $F(x, y, z, t) = 0$ and consists partly of the wall of the channel and partly of the free surface of the fluid. Hence the kinematic boundary condition can be written

$$\mathrm{D}_3 F = 0. \tag{A 4}$$

At the free surface $z = \eta(x, y, t)$ we have the dynamical condition

$$p(x, y, z = \eta, t) = p_s, \tag{A 5}$$

where p_s is the pressure over the surface. We define the cross-sectional and the free-surface averages of a function $f = f(x, y, z, t)$ by

$$\bar{f} = \frac{1}{S}\int_S \int f \,\mathrm{d}y\,\mathrm{d}z, \quad \tilde{f} = \frac{1}{b_2 - b_1}\int_{b_1}^{b_2} f(x, y, z = \eta, t)\,\mathrm{d}y,$$

where $y = b_1$ and $y = b_2$ denote the lateral positions of the shoreline or channel walls.

By integrating (A 2) over the cross-section of the channel and using the boundary condition (A 4) we obtain

$$\mathrm{D}S = -S\bar{u}_x, \tag{A 6}$$

where the operator D is as defined in §2. From (A 1)–(A 3) we get

$$u - \bar{u} = O(\epsilon), \quad \eta - \tilde{\eta} = O(\epsilon), \quad \eta - \bar{\eta} = O(\epsilon), \quad p = p_s + \eta - z + O(\epsilon). \tag{A 7}$$

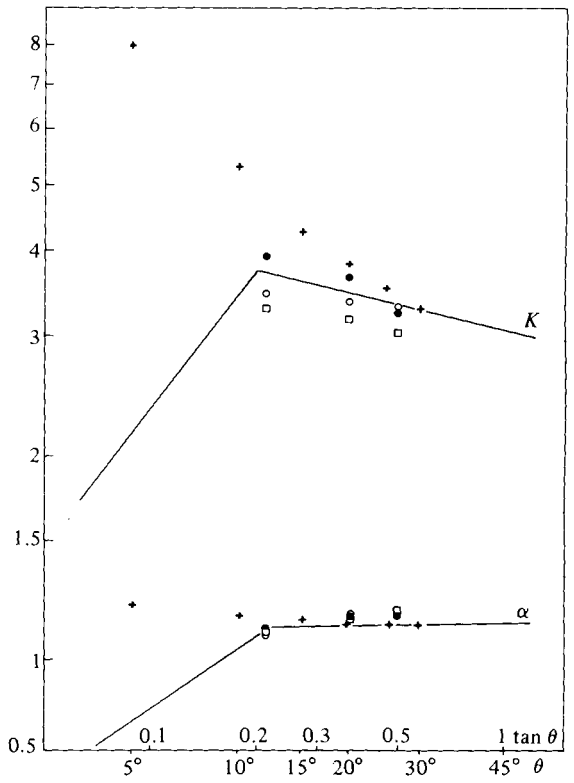

FIGURE 7. Experimental and theoretical (numerical) values of K and α (4.1) for different values of θ. Full drawn lines show experimental results by Hall & Watts; ●, ○ and □, Langsholt's experimental data for water depth $h = 25$ cm, 15 cm and 10 cm respectively; + + + +, results of numerical simulations.

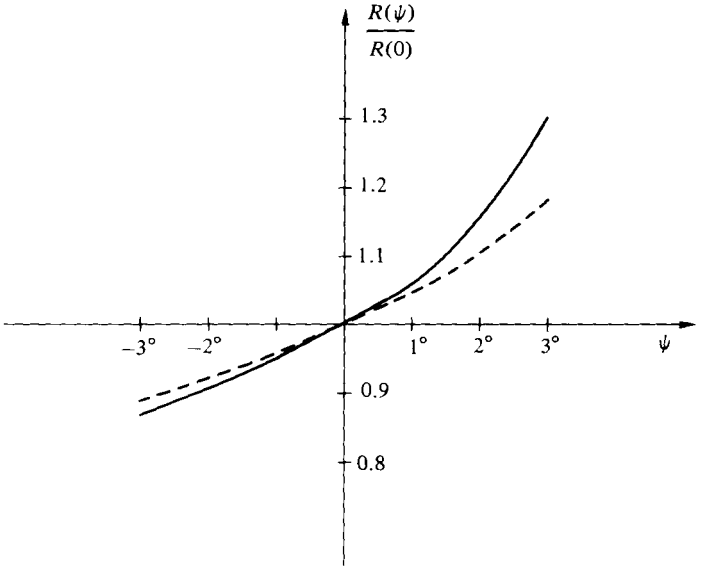

FIGURE 8. Run-up heights $R(\psi)$ for solitary waves in diverging ($\psi < 0$) and converging ($\psi > 0$) channels (relative to run-up height $R(0)$ in straight channel), ψ is the angle between the lateral walls and the longitudinal axis of the channel. $\theta = 15°$; ——, $A = 0.2$; – – – –, $A = 0.1$.

Equations (A 2)–(A 5) and (A 7) imply the existence of a potential ϕ such that $\phi_y = v + O(\epsilon)$ and $\phi_z = w + O(\epsilon)$ and

$$\nabla_1^2 \phi = -\bar{u}_x, \tag{A 8}$$

where $\nabla_1^2 = \partial^2/\partial y^2 + \partial^2/\partial z^2$. The kinematic boundary condition requires that the normal derivative

$$\frac{\partial \phi}{\partial n} = \frac{-\mathrm{D}F}{|\nabla_1 F|}, \tag{A 9}$$

where $\eta = \tilde{\eta}$ is substituted for the free-surface part of the boundary. $\nabla_1 F$ denotes the gradient vector in the (y, z)-plane. From the third equation of (A 1) we obtain by integration in the (y, z)plane

$$p = \tilde{p}_s + \tilde{\eta} - z + \epsilon(\tilde{E}_s - E) + O(\epsilon^2), \tag{A 10}$$

where $E = \mathrm{D}\phi + \frac{1}{2}(\nabla_1 \phi)^2$, and E_s is the value of E at the free surface $y = \tilde{\eta}$. The constant of integration had been determined from (A 5) by averaging. It can be shown that $u - \bar{u} = O(\epsilon)$ implies $\overline{(\mathrm{D}_3 u)} - \mathrm{D}\bar{u} = O(\epsilon^2)$. Hence from the first equation of (A 1) we find

$$\mathrm{D}\bar{u} = -(\tilde{p}_s)_x - \tilde{\eta}_x + \epsilon Q + O(\epsilon^2), \tag{A 11}$$

where $Q = \bar{E}_x - (\tilde{E}_s)_x$.

It is possible to find explicit solutions of (A 8) with the boundary condition (A 9) in special cases. For a channel with a rectangular cross-section defined by $b_1 \leqslant y \leqslant b_2$, $z > -h$ the mean value $\bar{f} = f(z = \eta) + O(\epsilon^2)$ and

$$\phi = \frac{1}{2}\frac{\mathrm{D}\bar{H}}{H} z^2 + \left(\mathrm{D}\bar{\eta} - \frac{\mathrm{D}\bar{H}}{H}\bar{\eta}\right) z + \frac{1}{2}\frac{\mathrm{D}(b_1 + b_2)}{b_1 + b_2} y^2 + \frac{b_1 \mathrm{D}b_2 - b_2 \mathrm{D}b_1}{b_1 + b_2}, \tag{A 12}$$

where $\bar{H} = \bar{\eta} + h$. The corresponding expression for K is given in (2.3).

For a channel with triangular cross-section the expression for ϕ is (Pedersen, 1981)

$$\phi = \frac{1}{2}\frac{\mathrm{D}H_m}{H_m} z^2 + \left(\mathrm{D}\tilde{\eta} - \frac{\mathrm{D}H_m}{H_m}\tilde{\eta}\right)\zeta + \frac{1}{2}\left(\frac{\mathrm{D}H_m}{H_m} - \frac{\mathrm{D}\beta}{\beta}\right) y^2,$$

where $H_m = h_m + \tilde{\eta}$, and h_m is the maximum depth in the undisturbed state. The slopes of the sides may vary in the longitudinal direction of the channel provided the ratio of the slopes is constant. The slope of one of the sides is denoted by β, and we note that the ratio of the slopes does not appear in the expression for ϕ.

Appendix B

The Lagrangian description is simplified by the fact that the flow is nearly one-dimensional. The only velocity appearing in the equations is the averaged horizontal velocity $\bar{u}$. Only one Lagrangian coordinate a is therefore needed. The definition of a is

$$\mathrm{D}a \equiv \frac{\partial a}{\partial t} + \bar{u}\frac{\partial a}{\partial x} = 0 \quad (t > 0), \quad a(x, 0) = 0. \tag{B 1}$$

Physically a may be interpreted as some mean initial position of the particles in a cross-section of the fluid. From (B 1) we get a simple but important relation for the individual derivative of a function f:

$$\mathrm{D}f = \mathrm{D}f(a, t) = \frac{\partial f(a, t)}{\partial a}\mathrm{D}a + \frac{\partial f(a, t)}{\partial t} = \frac{\partial f(a, t)}{\partial t}. \tag{B 2}$$

Applied to x, (B 2) immediately gives (2.4). Equation (2.2) is transformed to

$$S_t = -S\bar{u}_a/x_a. \tag{B 3}$$

This equation may be integrated in time to give

$$Sx_a = S_0(a), \tag{B 4}$$

where S_0 is the cross-sectional area at $t = 0$ and $x = a$. The more-standard form (B 3) is, however, often more suitable for numerical calculations, and (B 4) is therefore used mainly to eliminate the factor x_a which appears through transformation of x-derivatives. The transformation of the equation of motion is straightforward and the details are omitted.

REFERENCES

ARNTSEN, Ø. A. 1978 Theoretical and experimental study of wave run-up on relatively steep slopes. Cand.real. thesis, University of Oslo.

CARRIER, G. F. 1966 Gravity waves on water of variable depth. *J. Fluid Mech.* **24**, 641–659.

CARRIER, G. F. & GREEENSPAN, H. P. 1958 Water waves of finite amplitude on a sloping beach. *J. Fluid Mech.* **4**, 97–109.

CHANG, P., MELVILLE, W. K. & MILES, J. W. 1979 On the evolution of a solitary wave in a gradually varying channel. *J. Fluid Mech.* **95**, 401–414.

GJEVIK, B. & PEDERSEN, G. 1981 Run-up of long waves on an inclined plane. *Preprint Ser.* no. 2, *Dept of Maths, University of Oslo.*

HALL, J. V. & WATTS, G. M. 1953 Laboratory investigation of the vertical rise of solitary waves on impermeable slopes. *U.S. Army, Corps of Engrs, Beach Erosion Board, Tech. Memo* no. 33.

HELAL BADAWI, S. 1981 Etude théorique de la réflexion des ondes de gravité de grande longueur d'onde relative sur les plages. Thesis, L'Université scientifique et médicale, Grenoble.

HIBBERD, S. & PEREGRINE, D. H. 1979 Surf and run-up on a beach: a uniform bore. *J. Fluid Mech.* **95**, 323–345.

KISHI, T. & SAEKI, H. 1967 The shoaling, breaking and run-up of the solitary wave on impermeable rough slopes. In *Proc. 10th Conf. Coastal Engng, Tokyo*, 1966. ASCE, New York.

LANGSHOLT, M. 1981 Experimental study of wave run-up. Cand.real. thesis, University of Oslo.

MESINGER, F. & ARAKAWA, A. 1976 Numerical methods used in atmospheric models. *GARP Pub. Ser.* no. 17, *WMO-ICSU, Geneva.*

MEYER, R. E. & TAYLOR, A. D. 1972 Run-up on beaches. In *Waves on Beaches and Resulting Sediment Transport* (ed. R. E. Meyer), pp. 357–411. Academic.

MILES, J. W. 1979 On the Korteweg–de Vries equation for a gradually varying channel. *J. Fluid Mech.* **91**, 181–190.

PEDERSEN, G. 1981 Run-up of solitary waves in channel. Cand.real. thesis, University of Oslo.

PEREGRINE, D. H. 1968 Long waves in a uniform channel of arbitrary cross-section. *J. Fluid Mech.* **32**, 353–365.

PETERS, A. S. 1966 Rotational and irrotational solitary waves in a channel with arbitrary cross-section. *Communs Pure Appl. Maths* **19**, 445–471.

SHUTO, N. 1967 Run-up of long waves on a sloping beach. *Coastal Engng in Japan* **10**, 23–38.

SPIELVOGEL, L. Q. 1976 Single wave run-up on sloping beaches. *J. Fluid Mech.* **74**, 685–694.

WIEGEL, R. L. 1964 *Oceanographical Engineering.* Prentice-Hall.